Comparative study of wire bond degradation under power and mechanical accelerated tests

Popok, Vladimir; Buhrkal-Donau, Steffen; Czerny, Bernhard; Khatibi, Golta ; Luo, Haoze; Iannuzzo, Francesco; Pedersen, Kristian

Published in:
Journal of Materials Science: Materials in Electronics

DOI (link to publication from Publisher):
10.1007/s10854-019-02050-0

Publication date:
2019

Document Version
Accepted author manuscript, peer reviewed version

Journal of Materials Science: Materials in Electronics
accepted manuscript - DOI: 10.1007/s10854-019-02050-0

Comparative study of wire bond degradation under power and mechanical accelerated tests

V.N. Popok[1,*], S. Buhrkal-Donau[1], B. Czerny[2], G. Khatibi[2], H. Luo[3], F. Iannuzzo[3], K.B. Pedersen[4]

Abstract

Degradation of wire bonds under accelerated power cycling tests is compared to that caused by mechanical high-frequency cycling for commercial power devices. Using micro-sectioning approach and optical microscopy it is found that the bond fracture under the mechanical cycling follows the same tendencies as that found under power cycling. Results of shear tests of the mechanically cycled bonds also agree well with the bond cracking tendencies observed by optical microscopy investigations. It is found that reduction of contact area of the wire at the bond/metallization interface due to the crack development follows the Paris-Erdogan law, which defines the degradation rate leading to wire lift-off. The results obtained on mechanical cycling in the current work also show good agreement with literature data on wire bond fracture under power cycling proving that main mechanism for wire lift-off failure is related to the mechanical stress development at the interface with metallization layer. The carried out study also creates a potential to further develop a high-frequency mechanical cycling into an alternative for reliability analysis of wire bonds. However, more studies have to be performed to compare degradation mechanisms occuring under power and mechanical accelerated tests.

* V.N. Popok

vp@mp.aau.dk

[1] Department of Materials and Production, Aalborg University, Skjernvej 4A, 9220, Aalborg, Denmark

[2] Christian Doppler Laboratory for Lifetime and Reliability of Interfaces in Complex Multi-Material Electronics, Chemical Technology and Analysis, TU Wien, Getreidemarkt 9/CT-164, 1060 Vienna, Austria

[3] Department of Energy Technology, Aalborg University, Pontoppidanstræde 111, 9220 Aalborg, Denmark

[4] Converter Electrical, Power Solutions, Vestas Wind Systems A/S, Hedeager 42, 8200 Århus, Denmark

1 Introduction

Despite new emerging technologies for electrical connection of semiconductor dies in power modules, for example use of Cu wires [1], heavy Al wire bonds are still a dominating industrial method because it is technically well-established, cheap and it provides acceptable reliability. However, fatigue of wire bonds is one of the main factors limiting the device lifetime especially under conditions of variable load. Therefore, there is a continuous search for methods and models of trusty lifetime prediction.

Coffin-Manson model, which was initially developed to consider cyclic thermal stresses in solid state materials [2, 3], has been applied for decades as a relatively simple approach for lifetime estimation in the cases of thermally-induced degradation. In this approach, a number of cycles to failure is calculated as a function of temperature swings (ΔT) [4]. To improve estimations, it can also include an Arrhenius term with mean temperature [5] and other contributing parameters [6]. The weakness of this model is in use of fitting coefficients making it very difficult to transfer the reliability predictions to another type of device or even different operation conditions of the same device.

The other approach is based on physics of failure (PoF) analysis. It also has a history of a few decades [7]. In the recent years, PoF has been becoming more and more popular due to better reliability estimates [8-10]. Using this methodology, physical origins of the failure development are studied, thus, providing knowledge on the key stressors affecting the device degradation and leading to the end of life (EOL). This approach ensures deep understanding of the reliability aspects and easier transfer to different load conditions and diverse device configurations. A good example of PoF method in application to wire bond fatigue is presented in [11, 12] where the key factors affecting the degradation are estimated using a finite element based computational model and then experimentally verified.

Thus, PoF approach allows to design accelerated tests for distinct failure modes and distinguish between different degradation mechanisms. In line with this approach, there are tendencies to develop novel types of accelerated tests allowing to justify contributions of particular failure modes and to limit the analysis to one or very few degradation parameters. One of them is a passive thermal cycling, where the components of power modules are subjected to varying temperature on a short time scale without applying electric power [13, 14], thus, mimicking active power cycling but only in terms of thermal-induced stresses. Another approach suggests to utilize mechanical cycling of wire bonds in order to originate the stresses similar to those caused by the thermal-induced ones [15-17]. This mechanical cycling can be carried out at high frequencies reducing the test period to seconds and, thus, making it very attractive for reliability analysis. However, moving from accelerated power to mechanical tests requires thorough understanding of physics phenomena in both cases and careful comparison of undergoing degradation mechanisms.

In this paper, the possibility to reduce accelerated power tests, inducing thermo-mechanical stresses, to mechanical high-frequency cycling, originating only pure shear stresses, is further studied

by comparison of wire bond degradation for these two cases in order to see to what extent the mechanical tests can substitute the power ones.

2 Experimental

2.1 Samples and characterisation

In this work commercial power modules (30A, 600V) were studied. Every module consists of 6 equivalent sections comprising diode and IGBT chips with the metallization layers and bonded wires.

For the power accelerated tests, the devices were used almost as is, only top plastic cover was removed to reach desired electrical terminals and to monitor the temperature. For the mechanical tests, the silicone gel was additionally dissolved in order to get access to the wire bonds. The power cycled devices are noted with letter P, while the mechanically cycled ones with letter M further in the text.

For characterization of wire bonds, a micro-sectioning method was utilised. The devices were disassembled and silicone gel was removed (for the case of power cycled modules). Then, the samples were embedded into an epoxy, individual sections were mechanically cut to separate IGBT chips, which were then subjected to a series of mechanical operations involving grinding, polishing and, for some samples, electro-etching. One can find more details about these operations in [18]. Desired bonds were reached by polishing and images were obtained by optical microscopy. For the mechanically cycled samples subjected to shear tests, the foot prints after wire replacement were also imaged using scanning electron microscopy (SEM).

2.2 Power and mechanical cycling

Under the power cycling, DC current (I) pulses were applied to IGBTs of sections 1 and 6, S1 and S6. By varying I and on/off times (t_{on}/t_{off}) one can reach a desired mean junction temperature (T_j) and its variation (ΔT_j) which was measured using OTG-F-10 optical sensor (by OpSens). To monitor the wire bond degradation, collector-emitter voltage (V_{ce}) was recorded and the device was taken from the test when V_{ce} was increased to a certain value, which was measured in % with respect to initial V_{ce} of an uncycled device. Three modules were under evaluation in the current work. The test conditions are summarized in Tab. 1.

Details on the accelerated mechanical fatigue testing of the wire bonded interconnects has been presented earlier in [17]. It was conducted using Bondtec BAMFIT bonder / tester 5600 equipment. During the mechanical cycling the device was fixed on a vacuum stage, the tweezers grippers were aligned to the wire bond and pinched the wire. The cyclic shear loading was induced by exciting the grippers at constant displacement amplitude and frequency until a wire lift-off occurred, which was

detected by a height sensor. The displacement amplitude of the bonded area was measured by laser Doppler vibrometer [17]. In this study, the tests were conducted at a displacement amplitude of 360 nm and frequency of ~60 kHz with the mean number of cycles to lift-off failure being 1.2 Mcycles which is considered as EOL. A number of wire bonds were cycled to reach certain degradation stages between 10-90 % of EOL and then analysed by micro-sectioning to visualise cracking at the bond interface and to find out the remaining contact length, i.e. the wire fraction along the heel-toe direction, which was still bonded to the metallization layer. For the cases of lower (10-45) percentage of EOL, 4-6 wires were studied for each cycling condition, while for the cases of higher (60-90) percentage the number of analysed wires was increased to 8-12 to obtain better statistics. Initial contact length at wire-metallization interfaces was found to be approximately 700±50 μm for uncycled bonds. This uncertainty is related to variation in bond process of individual units.

2.3 Shear tests

Shear strength of the unstressed Al wire bonds and those subjected to mechanical fatigue testing was determined by Bondtec 5600 series bond shear tester with a testing speed of 300 μm/s and height of 20 μm. The average value of shear strength of the initial (uncycled) wire bonds was found to be 1160±30 cN. The shear tests on fatigued samples were conducted in order to determine the dependency of the bond strength on the degradation degree of the interface. Furthermore, the remaining contact area /length of the fatigued samples was measured using the foot print images of the sheared samples.

3 Results and discussion

It is well known that the degradation of wire bonds is started with micro-crack formation phase (stage 1) followed by the crack propagation through granular structure of interface (stage 2) and finalised by complete rupture (stage 3). For the current accelerated tests one can expect the majority of samples to be at stage 2 with some of them close or reaching stage 3. The degradation rate is expected to follow the Paris-Erdogan law [19]

$$da/dN = C\Delta K^m, \quad (1)$$

where da/dN is the propagation rate per cycle, C and m are the Paris' constants and ΔK is the stress intensity factor variation. Based on this law, it can be expected that the crack development will also follow a power law with a certain m. This tendency was earlier found for the same type of devices as in this work but subjected to passive thermal cycling [16].

As can be seen in Tab. 1, cycling of module P1 at current of 23 A led to relatively quick (149 kcyles) increase of V_{ce} above 6%. Therefore, module P2 was cycled at lower current of 22 A aiming at lower degradation level, which was reached for S1, ΔV_{ce} = 2.4 %. However, P2/S6 still showed V_{ce} increase above 6%. For module P3, the current was further reduced to 18 A. But in order to speed up the test, t_{on} was increased to 2.5 s. This change of cycling parameter increased ΔT but allowed to obtain ΔV_{ce} of about 2 % for 444 kcycles. Thus, we expect the sections of P3 as well as section 1 of P2 to demonstrate lower degradation of wire bonds compared to the other tested sections.

Micro-sectioning analysis of wire bonds on P3/S1 shows that the cracks develop from both sides (toe and heel) of the wires (see an example in Fig. 1(a)). There is still a considerable intact area at the wire/metallization interface that is in good agreement with the cycling conditions showing only 1.9 % of V_{ce} increase. Closer look into the crack structure (see Fig. 1(b)) leads us to conclusion that the fracture starts propagating through a boundary between the refinement area of the wire, where the grain size is changed under the bonding, and the unreconstructed part of the wire (with larger grains). This kind of fracture is quite typical and was earlier observed elsewhere [20]. However, under the further degradation, the cracks have tendency to develop towards the metallization and propagate exactly at the interface (see Fig. 1(b)). This type of crack evolution is observed for the majority of studied wire bonds and it is different from that found elsewhere where the fracture kept developing along the refinement area boundary [12]. Actually, for the case of current bonds the refinement areas are observed to be small and not well distinguishable. It is possible that the wires are slightly "underbonded", in the sense that wire and metallization do not become interconnected to appropriate level, therefore, we observe this unusual tendency in fraction development.

Wire bonds of P3/S6 (ΔV_{ce} = 2.2 %) and P2/S1 (ΔV_{ce} = 2.4 %) show similar delamination to that of P3/S1. One example is shown in Fig. 2(a). For the sections with ΔV_{ce} over 6%, the remaining contact areas are either very small (see Fig. 2(b)) or the wires are completely detached (Fig. 2(c)). Thus, one can conclude that such condition corresponds (or is very close) to EOL (complete bond rupture - stage 3). The fracturing occurs from both sides of wire bond but cracks on the toe side are typically more extensive for the majority of examined cases for this particular type of module. This dominating fracture development from toe side can be one more indication of not perfectly adjusted bonding procedure.

Micro-sectioning results of the mechanically-cycled samples show that the bonds corresponding to early degradation state (10-30 % of EOL) look very similar to those of the power cycled ones. The cracks are developed from both sides, i.e. heel and toe, with tendency to propagate through the boundary of the refinement area in the wire. For this early stage of wire bond damage, the crack length is small and contact length is large. An example of wire bond cross-section is shown in Fig. 3. With increasing number of cycles, i.e. percentage of EOL, crack length increases; they propagate towards each other until complete wire lift-off occurs. It is also observed for the majority of samples that the cracks, which are initiated at the refinement area boundary, are then tended to deviate towards the metallization in a

similar way to the case observed for the power cycled devices. The remaining contact length is measured using micro-sectioning images and the obtained results are presented as function of EOL percentage in Fig. 4(a). This dependence illustrates gradual degradation of wire bond interfaces and it is in very good agreement with shear tests for M samples presented in Fig. 4(b). One can see that the force is a decreasing function of EOL percentage because the contact length of wire bonds becomes smaller under increasing number of mechanical cycles. An example of remaining contact area (foot print) after the shear test of M device is shown in Fig. 5.

In order to compare the observed dependences with earlier data, the remaining length presented in Fig. 4(a) is normalized to the contact length of undamaged bond interface, thus, obtaining a relative length as function of EOL as shown in Fig. 6. This dependence can be fitted by power law (dashed line) of following type

$$y = a + bx^m, \tag{2}$$

were y corresponds to the relative remaining length, x is the EOL, a and b are the fit coefficients and m is the power, which is negative in this case because the remaining length should decrease with increasing EOL percentage. Therefore, eq. (2) is in agreement with eq. (1) and one can conclude that the fracture of wire bonds under the mechanical cycling follows the general tendency predicted by the Paris-Erdogan law. Unfortunately, the limited number of power-cycled samples in the current work does not allow us to draw the same conclusion. However, a number of cases of passive and active thermal cycling were extensively studied in literature, see for example [21-23], and we were able to find an reliability investigation of wire bonds similar to ours, to which we will refer below.

An important point for comparing bond degradation under mechanical and power cycling is to provide an appropriate transition between the two methods. This can be done using the procedure presented in [15], where the interfacial stress under the mechanical cycling was put in relation with the one caused by thermal processes allowing to find an equivalent temperature range for particular conditions of mechanical test. Using finite-element modelling, plots of so-called von Mises stress are calculated for the interfaces of Al wire bonds subjected to mechanical cyclic loading with amplitude of 360 nm, i.e. the condition of the current mechanical cycling. The average von Mises stress at the interfacial area near both ends of the wedge is found to be in the range of 36–37 MPa, which corresponds to an equivalent temperature range of about 70 C [15]. Thus, using the results presented in [22], where the crack growth for Al wire bonds with a diameter of 300 μm (similar to our case) was studied at ΔT of 75 C, we are able to add the data of power cycling to our plot presented in Fig. 6. These data show a very good correlation with power law fit line representing the M samples. It is worth mentioning that the given equivalent ΔT = 70 °C should be considered as a first approximation. A more accurate value for the equivalent temperature range requires further thermo-mechanical simulations.

However, the obtained agreement confirms the primary aim of this work and demonstrates the similarity in wire bond fatigue under accelerated thermal and mechanical tests.

4 Conclusions

Degradation of wire bonds under both accelerated power cycling and pure mechanical high-frequency cycling is studied and compared. It is found that the damage introduced by the mechanical cycling follows the same tendency as that observed under the power cycling, namely: the bond fracture is developed from both the heel and toe sides of wire; the cracks start propagating in the wire through the boundary of refinement area; with increase of degradation level the fracture deviate towards metallization interface and cracking on the toe side becomes much more extensive. Such way of degradation can be explained by not perfectly optimised bonding procedure for the devices under the study.

The analysis of remaining contact length as a function of EOL for the mechanically-cycled samples shows the power law dependence allowing us to apply well-known physical laws of fracture mechanics, in particular the Paris-Erdogan law, for bond fatigue, thus, bringing a basis for use of PoF approach in lifetime prediction. The power law dependence obtained under the pure mechanical cycling shows a good agreement with the literature data found on similar bonds subjected to power cycling. This finding indicates that the mechanical stresses induced under a power cycling (through expansion/contraction related to heating/cooling, respectively) are the main driving forces for bond degradation and fracture development. Thus, high-frequency mechanical cycling has a potential to be developed into an alternative for reliability analysis of wire bonds. However, this approach still requires more studies on different types of wires accompanied by analysis of phenomena on the microscale.

Acknowledgements

This work is part of the activities run at the Center of Reliable Power Electronics (CORPE) in Denmark. The financial support by the Austrian Federal Ministry for Digital and Economic Affairs and the National Foundation for Research, Technology and Development is gratefully acknowledged.

References

1. P.S. Chauhan, A. Choubey, Z. Zhong, M.G. Pecht, *Copper Wire Bonding* (Springer, 2014).
2. L. F. Jr. Coffin, Trans. ASME **76**, 931-950 (1954).

3. S. S. Manson, Proceedings Heat Transfer Symposium, University of Michigan 9-75 (1953)
4. M. Ciappa, Microelectron. Reliabil. **42**, 653-667 (2002).
5. M. Held; P. Jacob; G. Nicoletti; P. Scacco; M.-H. Poech, Proceedings 2nd International Conference on Power Electronics and Drive Systems 425-430 (1997), DOI: 10.1109/PEDS.1997.618742
6. U. Scheuermann, R. Schmidt, Microelectron. Reliabil. **53**, 1687-1691 (2013).
7. G.H. Ebel, IEEE Trans. Reliabil. **47**, SP379-389 (1998).
8. Z. Matic, V. Sruk, Proceedings of 30th International Conference on Information Technology Interfaces 745-750 (2008), DOI: 10.1109/ITI.2008.4588504
9. C. Hendriks, E. George, M. Osterman, M. Pecht, in *Reliability Characterisation of Electrical and Electronic Systems*, Ed. J. Swinger (Elsevier, 2015) pp. 27-42.
10. H. Wang, M. Liserre, F. Blaabjerg, P. de Place Rimmen, J. B. Jacobsen, T. Kvisgaard, J. Landkildehus, IEEE J. Emerg. Sel. Top. Power Electron. **2**(1), 97–114 (2014).
11. K. B. Pedersen, K. Pedersen, IEEE Trans. Power Electron. **31**, 975–986 (2016).
12. V.N. Popok, K.B. Pedersen, P.K. Kristensen, K. Pedersen, Microelectron. Reliab. **58**, 58-64 (2016).
13. M. Brincker, K.B. Pedersen, P.K. Kristensen, V.N. Popok, Microelectron. Reliabil. **55**, 1988-1991 (2015).
14. M. Brincker, K.B. Pedersen, P.K. Kristensen, V.N. Popok, IEEE Transact. Components Packaging Manufact. Technol. **8**(12), 2073-2080 (2018).
15. B. Czerny, G. Khatibi, Microelectron. Reliabil. **58**, 65-72 (2016).
16. K.B. Pedersen, D.A. Nielsen, B. Czerny, G. Khatibi, F. Iannuzzo, V.N. Popok, K. Pedersen, Microelectron. Reliabil. **76-**77, 373-377 (2017).
17. B. Czerny, G. Khatibi, Technisches Messen, **85**(4) (2018) 213-220.
18. K.B. Pedersen, P.K. Kristensen, V. Popok, K. Pedersen, Microelectron. Reliabil. **53**, 1422-1426 (2013).
19. N. Pugno, M. Ciavarella, P. Cornetti, A. Carpinteri, J. Mech. Phys. Sol. **54**(7), 1333-1349 (2006).
20. K. B. Pedersen, D. Benning, P.K. Kristensen, V.N. Popok, K. Pedersen, J. Mater. Sci.: Mater. Electron. **25**, 2863-2871 (2014).
21. L. Yang, P. Agyakwa, C. M. Johnson, IEEE Trans. Device Mater. Reliabil. **13**, 9-17 (2013).
22. Grams, J. Höfer, A. Middendorf, S. Schmitz, O. Wittler, K.-D. Lang, Proceedings 16th International Conference on Thermal, Mechanical and Multi-Physics Simulations and Experiments in Microelectronics and Microsystems (2015), DOI: 10.1109/EuroSimE.2015.7103091.
23. K. Sasaki, N. Iwasa, T. Kurosu, K. Saito, Y. Koike, Y. Kamita, Y. Toyoda, Proceedings 20th International Symposium on Power Semiconductor Devices and ICs 181-184 (2008), DOI: 10.1109/ISPSD.2008.4538928

Table 1

Power cycling conditions

Module/ section	I (A)	t_{on}/t_{off} (s)	$T_j/\Delta T_j$ (°C)	kcycles	ΔV_{ce} (%)
P1/S1	23	1.5/1.5	80/40	149	6.4
P1/S6	23	1.5/1.5	80/40	149	6.3
P2/S1	22	1.5/1.5	80/40	406	2.4
P2/S6	22	1.5/1.5	80/40	406	6.9
P3/S1	18	2.5/2.5	80/60	444	1.9
P3/S6	18	2.5/2.5	80/60	444	2.2

Figure captions

Figure 1. Optical images of a wire bond obtained by micro-sectioning of P3/S1 (a) before and (b) after electro-etching. Image (b) shows only heel of bond.

Figure 2. Optical images of wire bonds obtained by micro-sectioning of (a) P3/S6, (b) P1/S1 and (c) P2/S6.

Figure 3. Optical image of wire bond mechanically cycled to 30 % of EOL.

Figure 4. (a) Remaining length of wire bonds subjected to mechanical cycling and (b) shear force applied to remove bonds as function of EOL.

Figure 5. SEM image of foot prints after the shear test. The wire bonds were mechanically-cycled to 45% of EOL.

Figure 6. Relative remaining length of wire bonds subjected to mechanical cycling, which is fitted by power law, in comparison to the power cycling data from [22]. Error bars show standard deviations.

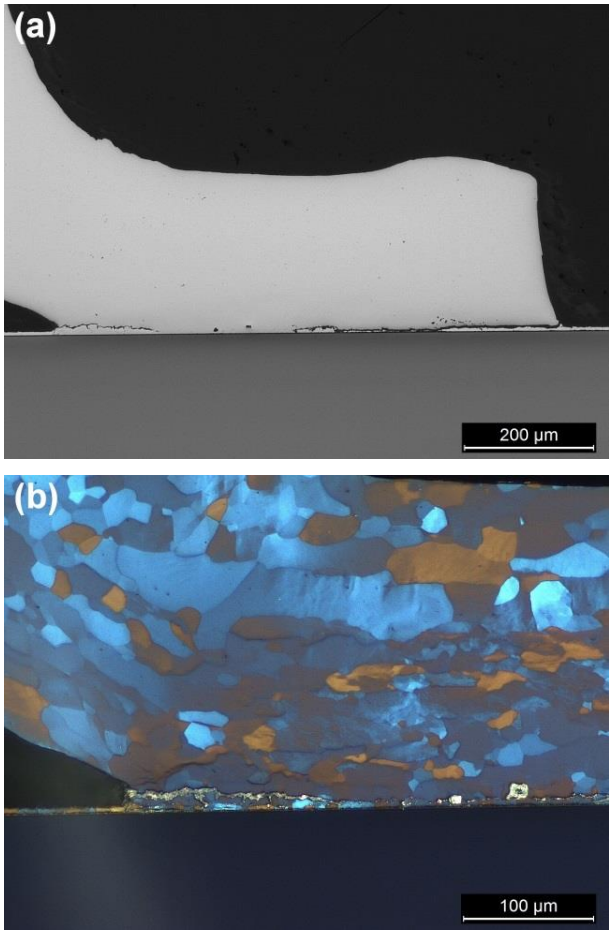

Fig. 1

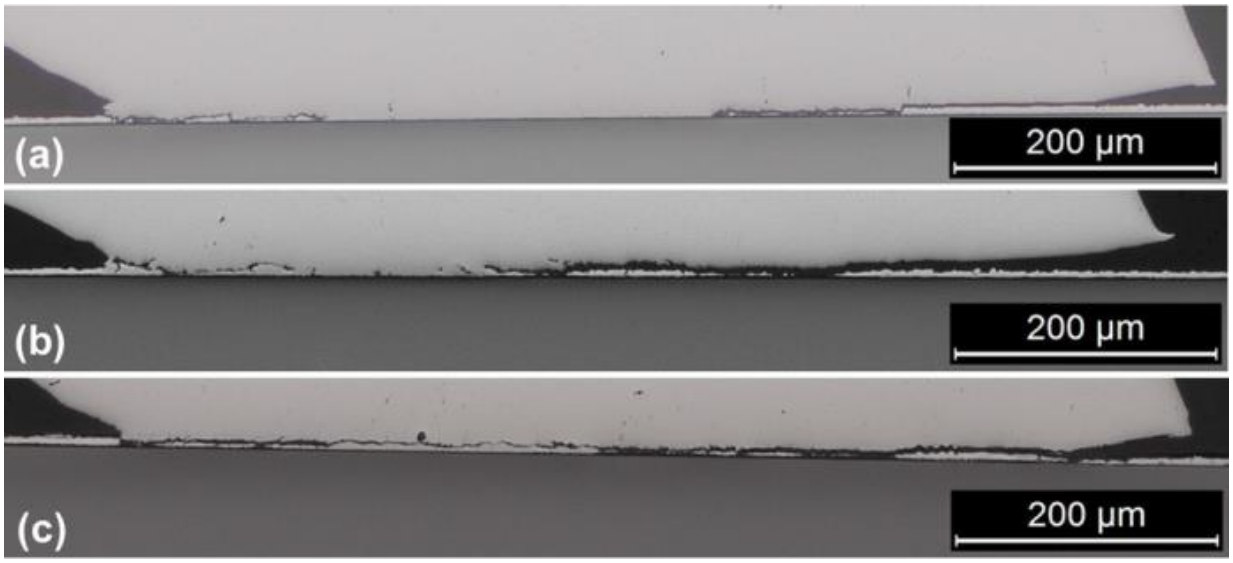

Fig. 2

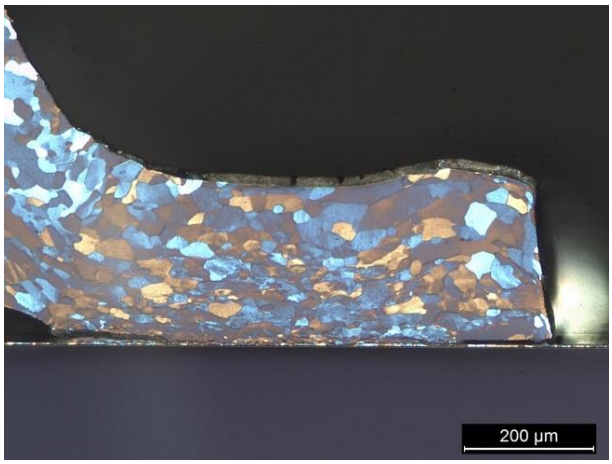
200 µm

Fig. 3

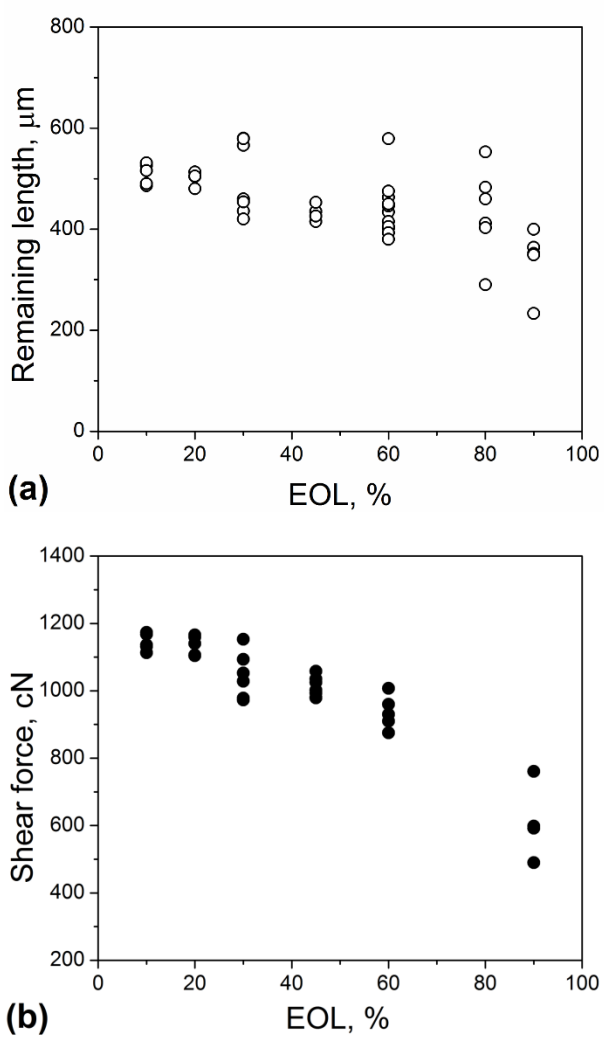
Remaining length, µm
0
200
400
600
800
0
20
40
60
80
100
EOL, %
(a)
Shear force, cN
200
400
600
800
1000
1200
1400
0
20
40
60
80
100
EOL, %
(b)

Fig. 4

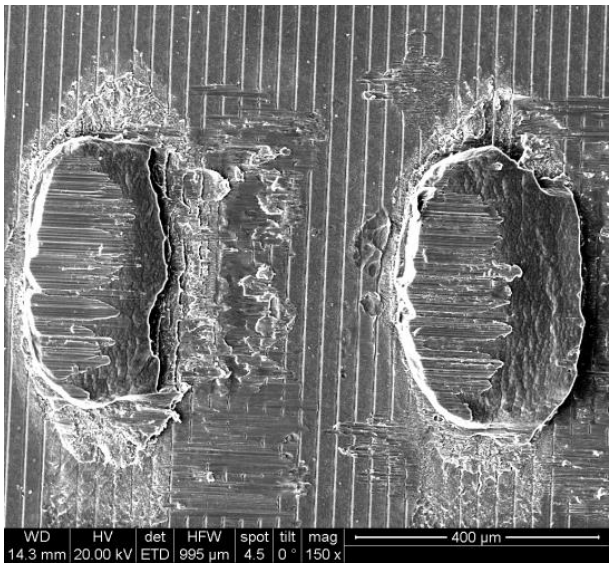
WD
14.3 mm
HV
20.00 kV
det
ETD
HFW
995 µm
spot
4.5
tilt
0 °
mag
150 x
400 µm

Fig. 5

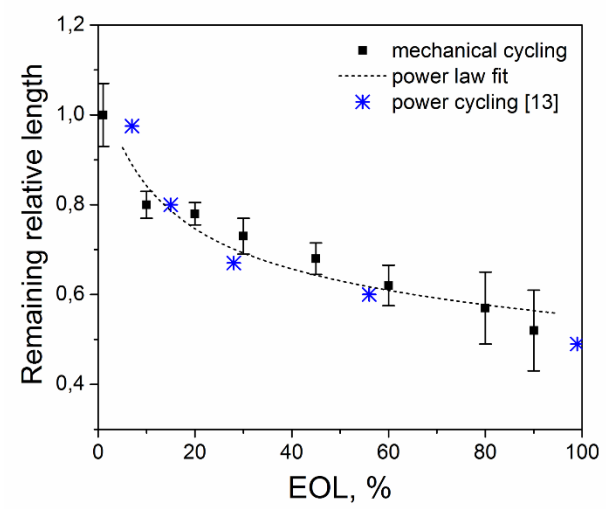
mechanical cycling
power law fit
power cycling [13]
Remaining relative length
EOL, %
1,2
1,0
0,8
0,6
0,4
0
20
40
60
80
100

Fig. 6